Volume 57
Number 90
21 November 2021
Pages 11875–12034

ChemComm

Chemical Communications

rsc.li/chemcomm

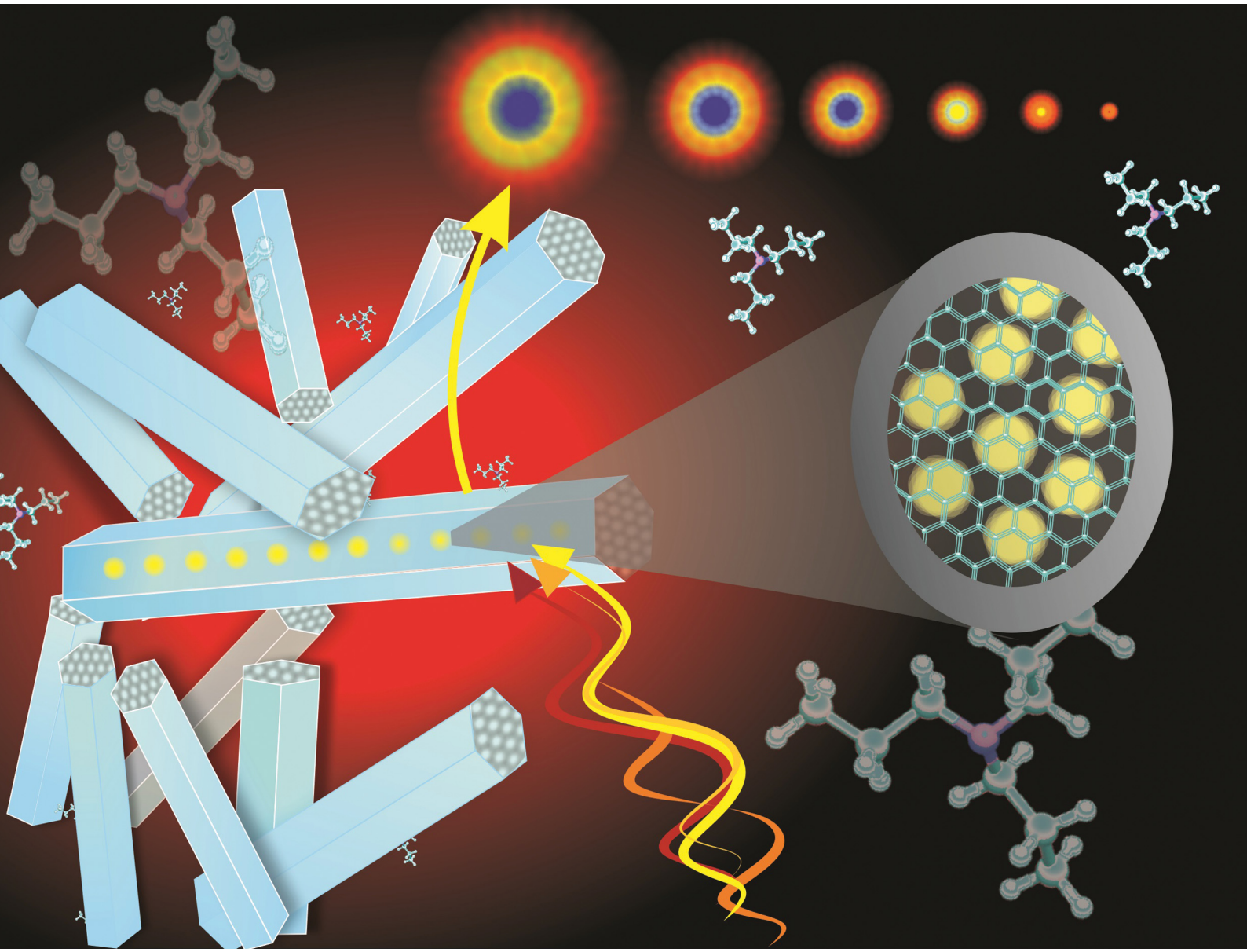

ISSN 1359-7345

ROYAL SOCIETY OF CHEMISTRY

COMMUNICATION

Eduardo Coutino-Gonzalez *et al.*

Optical encoding of luminescent carbon nanodots in confined spaces

ChemComm

COMMUNICATION

View Article Online
View Journal | View Issue

Cite this: *Chem. Commun.*, 2021, **57**, 11952

Received 26th August 2021,
Accepted 15th October 2021

DOI: 10.1039/d1cc04777a

rsc.li/chemcomm

Optical encoding of luminescent carbon nanodots in confined spaces†

Evelyne Bartholomeeusen,[a] Gert De Cremer,[b] Koen Kennes,[c] Ceri Hammond,[d] Ive Hermans,[e] Jiang-bo Lu,[fg] Dominique Schryvers,[g] Pierre A. Jacobs,[a] Maarten B. J. Roeffaers,[h] Johan Hofkens,[c] Bert F. Sels[a] and Eduardo Coutino-Gonzalez*[i]

Stable emissive carbon nanodots were generated in zeolite crystals using near infrared photon irradiation gradually converting the occluded organic template, originally used to synthesize the zeolite crystals, into discrete luminescent species consisting of nano-sized carbogenic fluorophores, as ascertained using Raman microscopy, and steady-state and time-resolved spectroscopic techniques. Photo-activation in a confocal laser fluorescence microscope allows 3D resolved writing of luminescent carbon nanodot patterns inside zeolites providing a cost-effective and non-toxic alternative to previously reported metal-based nanoclusters confined in zeolites, and opens up opportunities in bio-labelling and sensing applications.

Several strategies for the optical encoding of microcarriers have been applied in multiplex bio-assays or in encoding compound libraries synthesized using combinatorial chemistry.[1–3] Aside from labeling purposes, microcarriers are increasingly used in the fields of drug discovery, drug screening and medical diagnostics.[3–6] Optical encoding strategies usually employ organic fluorescent tags entrapped into the microbeads beforehand, which limits the variety of codes available.[2] Furthermore, differential photobleaching and leaching of the fluorophore from the microcarrier body restrict their use. Whereas various labelling strategies are based on the encoding of microcarriers beforehand, also referred to as ''fixed encoding'', it is more advantageous to have an active or *in situ* encoding method, wherein the encoding is conducted during the experiment. Such an approach would give a virtually unlimited variety of unique codes that can be created during a microscopic assay. Braeckmans and collaborators demonstrated the feasibility of this technique by using spatially-resolved selective photobleaching, which resulted in negative contrast codes.[7] On the other hand, positive contrast strategies have been developed using X-rays or photo-induced activation protocols in silver-exchanged zeolites and MOFs.[8–10] Despite the high brightness of the encoded patterns and their ease of processing, the risk of silver ions leaching from the zeolite framework may hinder their application in biocompatible experiments.[8] Carbon-based nanomaterials, *e.g.* graphene,[11–13] carbon nanotubes, nanofibers, and nanodots,[14–18] have gained interest as nanotags due to their biocompatibility. Moreover, porous inorganic materials such as zeolites have been employed for the preparation of luminescent carbon nanotubes and intraporous carbon deposits using thermal treatment of as-synthesized zeolite powders.[19–24] Upon heating, the organic template molecule decomposes according to the Hofmann elimination and subsequently forms carbogenic species in the pores of the zeolites.[25] While the structural details of the carbogenic species vary from graphene-like carbon to ultra-thin carbon nanotubes, the luminescence displayed by the carbon-loaded zeolite powder is bright with tunable wavelengths. Nevertheless, the on-purpose synthesis of individual luminescent sub-micrometer sized carbon species from organic precursors in zeolites has been poorly addressed. Herein, we report the generation of discrete luminescent carbon nanodots in well-defined AFI-type zeolite (AlPO-5) crystals *via* light-induced activation upon near infrared laser irradiation. By using this approach, luminescent metal-free zeolite microcarriers with clear contrast and multicolor abilities are created and result in highly resolved (submicron-sized) luminescent codes.

[a] *Chem&Tech – Centre for Sustainable Catalysis and Engineering (CSCE), KU Leuven, Celestijnenlaan 200F, B-3001 Leuven, Belgium*
[b] *DSM Protective Materials, PO Box 1163, 6160BD Geleen, The Netherlands*
[c] *Chem & Tech – Molecular Imaging and Photonics, KU Leuven, Celestijnenlaan 200F, B-3001 Leuven, Belgium*
[d] *Department of Chemical Engineering, Imperial College London, South Kensington, SW7 2AZ, London, UK*
[e] *Department of Chemistry & Department of Chemical and Biological Engineering, University of Wisconsin-Madison, 1101 University Av., Madison, WI 53706, USA*
[f] *School of Physics and Information Technology, Shaanxi Normal University, Xi'an, 710119, P. R. China*
[g] *EMAT, University of Antwerp, Groenenborgerlaan 171, B-2020 Antwerpen, Belgium*
[h] *Chem&Tech – Centre for Membrane Separations, Adsorption, Catalysis and Spectroscopy for Sustainable Solutions, KU Leuven, Celestijnenlaan 200F, B-3001 Leuven, Belgium*
[i] *Centro de Investigaciones en Óptica, A. C. Loma del Bosque 115, Colonia Lomas del Campestre, León, Guanajuato 37150, Mexico. E-mail: ecoutino@cio.mx*

† Electronic supplementary information (ESI) available: Additional information on the optical properties, encoding resolution and stability of the materials. See DOI: 10.1039/d1cc04777a

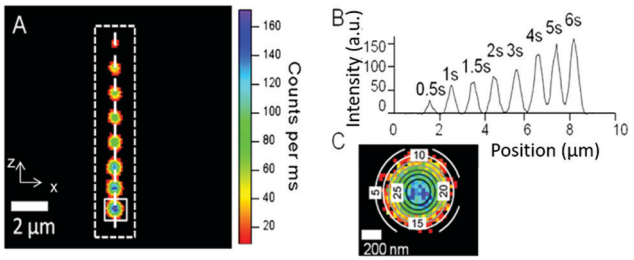

Fig. 1 Visualization of the photoluminescence after locally activating the carbon nanodots in an individual AlPO-5 crystal (the contour of the crystal is indicated by the dotted rectangle). Image of eight dots (A), and the intensity profile (B) along the dashed white line in image A. The corresponding activation times are displayed for each point, (C) shows a magnified image of a luminescent carbon nanodot, activated for 6 seconds, and the intensity profile fitted with a 2D Gaussian function (colored contour lines; FWHM,x = 452 nm).

Representative examples of the produced emissive carbon nanodots are shown in Fig. 1A. Eight dots were activated along the length of an individual AlPO-5 crystal (approximately $10 \times 2 \times 2$ µm^3), using a femtosecond pulsed 780 nm laser focused on the sample through a confocal fluorescence microscope (further details of the set-up and zeolite synthesis can be found in the ESI†). Activation was conducted in a droplet of water added on top of the zeolite crystals. Interestingly, in the presence of water significantly shorter activation times (up to a factor of 30) are required to obtain bright nanodots with similar intensities. This could be associated with the production of reactive species during water photolysis under UV irradiation affecting the surface chemistry of the formed carbon nanodots, as previously suggested.[26]

The presence of the tripropylamine (TPA) template molecule in the zeolite matrix is essential for the formation of the emissive dots. In contrast, zeolites that were calcined under air prior to photo-activation and thus free of the template molecule, did not show any photoluminescence in the visible range after local activation, revealing that indeed luminescent carbon species, and not structural oxygen defects, such as oxygen or vacancies in the zeolite,[27–29] are responsible for the displayed photoluminescence. In accordance with the known photo-stability of C-dot structures, the activated pattern (Fig. 1A) remains notably stable over an extended period of time under ambient conditions (see the ESI,† Fig. SI-3; tested after 3 months of storage under ambient conditions). Interestingly, contrast and brightness was readily introduced by controlling the photo-activation time, and created nanodots of different luminescence intensities. This is illustrated in Fig. 1B, where the intensity profile along the dashed white line is shown. In the experiment, the activation time of each individual dot was increased by 0.5 or 1 second. Clearly, when a spot on the zeolite is activated for a longer time, more organic template is transformed into the carbogenic fluorophore, which is reflected in the intensity profile. A more detailed view is presented in Fig. 2A, where the intensity is plotted as a function of the activation time for the case of three different AlPO-5 crystals.

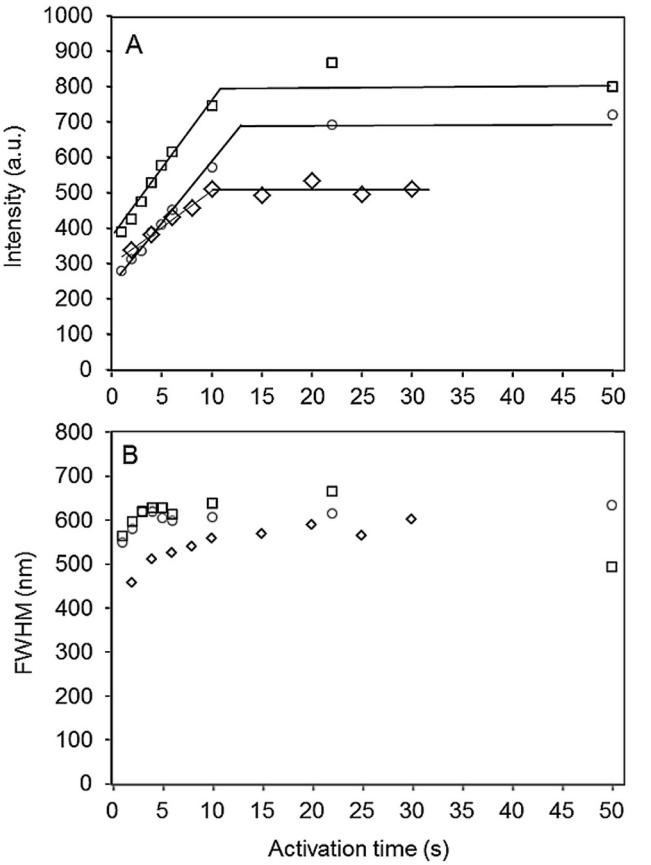

Fig. 2 Intensity (A) and FWHM (B) of photo-activated carbon nanodots, given as a function of the activation time for 3 individual AlPO-5 crystals using 9.5 MW cm^{-2} as the activation power. The solid lines in Fig. 2A are only used to indicate the trends.

The true spatial resolution of the bright spot was determined by fitting the experimentally recorded point spread function (PSF) of the intensity with a 2D Gaussian function. The PSF of an individual activated dot overlaid with the 2D Gaussian plot is shown in Fig. 1C. In Fig. 2B the FWHM is plotted as a function of the photo-activation time, and shows that the spot-size only slightly enlarges (about 10–20%) with the activation time. In spite of this slight increase, the resolution remains high and can even approach the theoretical resolution limit for two-photon excitation microscopy (see Fig. SI-5, ESI†),[14] which is indicative of a two-photon activation process. Confinement imposed by the zeolite pores suggests a restricted growth of the luminescent carbon nanodots parallel to the channel dimension of the zeolite pores as corroborated by polarization experiments (Fig. 3), which indicate that growth of the emissive carbon structures is stimulated mainly in the illuminated volume of the zeolite crystal.

The spectroscopic study of the bright carbon nanodots revealed a broad photoluminescence (PL) emission, which is typically observed for isolated carbon dots, for instance, synthesized using hydrothermal treatment of aqueous sugar solutions. Both the PL spectra and fluorescent lifetimes of a representative luminescent spot were analyzed under a 375 nm excitation light.

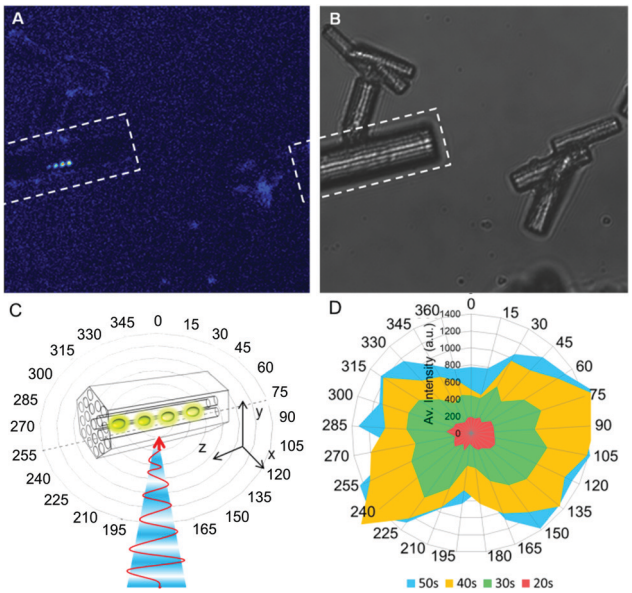

Fig. 3 Illustration of the fluorescence polarization of the bright spots formed in AlPO-5 using focused photo-activation. (A) Fluorescence and (B) transmission optical images of the irradiated crystal, denoted with a white rectangle. The red arrow indicates the polarization orientation of the 488 nm laser beam (C), and (D) the intensity plot of four distinct spots activated for 20 s (red), 30 s (green), 40 s (yellow) and 50 s (blue), at different rotation angles, demonstrating the polarization of the emission.

The results are displayed in the ESI† (Fig. SI-8 to SI-12). The observed emission maximum is centered between 570–590 nm. Deconvolution of the photoluminescence spectra, using the Gaussian function, was conducted to indicate the complex nature of the formed carbon nanodots revealing multiple emitters contributing to the observed emission color, and displayed bands centered at 530, 600, and 670 nm, respectively. The fluorescent lifetimes at the single crystal level, which can only be fitted adequately using a multi-exponential function, were analyzed using fluorescein as the internal reference, which has a known decay time of 3.97 ns (see Fig. SI-12, ESI†). Two characteristic decay times typically appear within the detection limit, with $\tau(1) = \sim 1$ ns, and $\tau(2) = \sim 4$–5 ns (see the ESI,† Table SI-I and S-II) with an average excited-state lifetime varying between 2 and 3 ns, which is comparable to the lifetimes of related carbon nanodots.[30] This behavior, the broad luminescence spectra and the exhibited multi-exponential decay, suggest the presence of multiple types of emitters or multiple environments in the single bright spot, and possibly also involves an energy transfer processes.[31] The different emission colors may be explained by the different sizes of the individual nano-sized emitters. However, experimental evidence purely based on the size-dependence of the optical properties in the literature should be interpreted with caution since photoluminescence is also affected by symmetry, defects and the environment in which the nanodots are confined. In principle, the dimensions of the nanodots cannot exceed (in two directions) the pore size of the zeolite host material in the *xy* direction, which has a diameter of 0.7 nm (see Fig. SI-2 in the ESI†). Propagation growth in the *z*-axis, along the pore direction, is a plausible hypothesis to explain the different emission maxima. However, we noted that the emission maxima did not change upon increasing the activation time from 1 to 10 seconds, although the emission intensity clearly increases (this is shown in Fig. SI-10 of the ESI†), and suggests that multiple species are formed simultaneously rather than a quantum confinement effect. Also the effect of the zeolite composition on the emission intensity and spectral behavior (lifetimes and emission maxima) was investigated. Similar to the photo-activated dots in AlPO-5, patterns were encoded in the related SAPO-5 zeolite structure. The Si sites in this framework that are coordinated to Al will give rise to a negative framework charge, which could influence the reaction chemistry by including Brønsted acidity. The photo-activation of carbon nanodots in the SAPO-5 zeolites is similar to that of the AlPO-5 zeolites; however, the emission intensity is notably reduced (see the ESI,† Fig. SI-10). The resulting fluorescent emitters exhibit a small, but clear blue shift of 33 nm in wavelength compared to AlPO-5 (see the ESI,† Fig. SI-8). This suggests that depending on the composition of the zeolite host, it might be possible to fine-tune the resulting emission colors.[9]

Further identification of the generated carbogenic fluorophores with Raman microscopy showed two signature peaks. The inset in Fig. 4 depicts a rather broad signal at around 1400 cm^{-1} in the D-band region and a sharper signal at 1606 cm^{-1} in the G-band region, which are related to the A1g zone edge breathing vibration phonon in the presence of a neighboring sp^3 defect and to the E2g in-plane stretching vibration mode of the sp^2 bonded carbon in a graphite lattice, respectively.[32,33] The small shift of the G-band from that of ideal crystalline graphene (1580 cm^{-1}) and the rather large D/G ratio, which is larger than unity, are indicative of a high proportion of disordered or defective regions being present in the carbogenic graphene-like structure.[34,35]

This suggests that the photo-activated bright spot is composed of both amorphous and graphitic-like carbon single emitters in the nanometer range.[36] The π states of the sp^2 carbon sites likely govern the photoluminescence behavior in

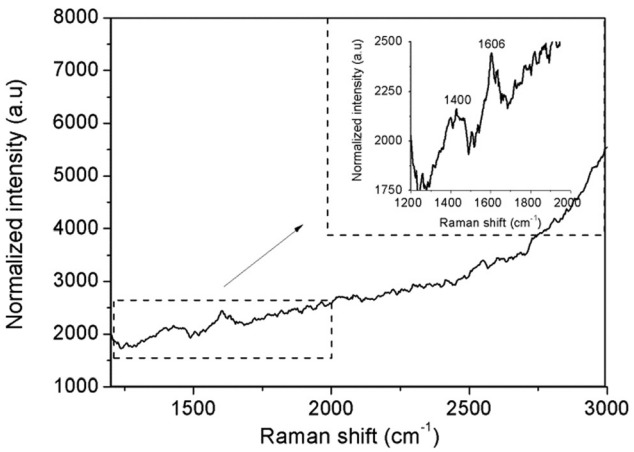

Fig. 4 Raman spectrum from 1200 to 3000 cm^{-1} of an activated carbon nanodot in AlPO-5 after background subtraction. The inset shows an enlargement of the observed D and G-bands.

such disordered graphite-like nanomaterials by photogeneration of electron–hole pairs, followed by radiative recombination.[37,38] The radial breathing modes, which are characteristic of the presence of carbon nanotubes as observed in thermo-activated zeolites powders at low Raman shifts (see the ESI,† Fig. SI-13, *e.g.* in the range of 400 to 600 cm^{-1}), were not observed in the emissive spot, but their complete absence may be due to the low sensitivity of the experiment. Advanced characterization of the composition and structure of the individual emitters is ongoing to underpin the origin of the carbogenic fluorophores.

The photo-activation approach used in this study is particularly suited to generating emissive carbon nanodots at distinct locations in single zeolite crystals, and makes use of the presence of organic template molecules. Transformation of the template molecules into emissive spots is restricted to the illuminated focal volume. The emissive spots consist of nano-sized carbon emitters confined within the zeolite host pores, where their density and thus the spot brightness is dependent of the illumination time. Identifying the nano-sized emitters in the bright spot using their spectral and vibrational behavior exposes similar characteristics to those reported for luminescent carbon nanodots. Whereas the growth mechanism remains unclear, the presence of other heteroelements, for instance Si, in the zeolite matrix, causes a shift of the emission band. Primarily consisting of carbon precursors and zeolite crystals, these materials provide a cost-effective, non-toxic, promising alternative for metal/dye-containing emissive micro-carriers. Furthermore, they are expected to interfere with biological specimens to a much lesser extent than metallic quantum dots in bio-imaging applications.

Conceptualization: G. De Cremer, M. B. J. Roeffaers, J. Hofkens, P. A. Jacobs, B. F. Sels and E. Coutino-Gonzalez. Investigation and formal analysis: E. Bartholomeeusen, K. Kennes, G. De Cremer, D. Schryvers, J. Lu, I. Hermans, C. Hammond, and E. Coutino-Gonzalez. Visualization: G. De Cremer, B. F. Sels, and E. Coutino-Gonzalez. Writing (original draft): all authors. Writing (review and editing): all authors.

This work was performed within the framework of the IAP-VI program for Supramolecular Chemistry and Catalysis of the Belgian Federal government. We gratefully acknowledge financial support from the Flemish government through an FWO research grant (G.0603.10N), the European Union's Seventh Framework Programme (FP7/2007-2013 under grant agreement n° 310651 SACS), and the CONACYT-CB funds (grant A1-S-44458).

Conflicts of interest

There are no conflicts to declare.

Notes and references

1 R. Wilson, A. R. Cossins and D. G. Spiller, *Angew. Chem., Int. Ed.*, 2006, **45**, 6104.
2 B. J. Battersby, D. Bryant and W. Meutermans, *et al.*, *J. Am. Chem. Soc.*, 2000, **122**, 2138.
3 M. Han, X. Gao, J. Z. Su and S. Nie, *Nat. Biotechnol.*, 2001, **19**, 631.
4 M. R. Carro-Tembury, R. Arppe, T. Vosch and T. J. Sørensen, *Sci. Adv.*, 2018, **4**, e1701384.
5 K. Braeckmans, S. C. De Smedt and M. Leblans, *et al.*, *Nat. Rev. Drug Discovery*, 2002, **1**, 447.
6 F. Fayazpour, B. Lucas and N. Huyghebaert, *et al.*, *Adv. Mater.*, 2007, **19**, 3854.
7 K. Braeckmans, S. C. De Smedt and C. Roelant, *et al.*, *Nat. Mater.*, 2003, **2**, 169.
8 G. De Cremer, B. F. Sels and J. Hotta, *et al.*, *Adv. Mater.*, 2010, **22**, 957.
9 E. Coutino-Gonzalez, D. Grandjean and M. B. J. Roeffaers, *et al.*, *Chem. Commun.*, 2014, **50**, 1350.
10 R. Ameloot, M. B. J. Roeffaers and G. De Cremer, *et al.*, *Adv. Mater.*, 2011, **23**, 1788.
11 G. Eda, Y. Y. Lin and C. Mattevi, *et al.*, *Adv. Mater.*, 2010, **22**, 505.
12 A. Nourbakhsh, M. Cantoro and T. Vosch, *et al.*, *Nanotechnology*, 2010, **21**, 435203.
13 L. Cao, M. J. Meziani, S. Sahu and Y. P. Sun, *Acc. Chem. Res.*, 2013, **46**, 171.
14 S. T. Yang, X. Wang and H. Wang, *et al.*, *J. Phys. Chem. C*, 2009, **113**, 18110.
15 L. Cao, X. Wang and M. J. Meziani, *et al.*, *J. Am. Chem. Soc.*, 2007, **129**, 11318.
16 S. T. Yang, L. Cao and P. G. Luo, *et al.*, *J. Am. Chem. Soc.*, 2009, **131**, 11308.
17 Z. L. Peng, E. H. Miyanji and Y. Q. Zhou, *et al.*, *Nanoscale*, 2017, **9**, 17533.
18 M. Bhatt, S. Bhatt and G. Vyas, *et al.*, *ACS Appl. Nano Mater.*, 2020, **7**, 7096.
19 Z. K. Tang, H. D. Sun and J. Wang, *et al.*, *Appl. Phys. Lett.*, 1998, **73**, 2287.
20 Z. M. Li, H. J. Liu and J. T. Ye, *et al.*, *Appl. Phys. A: Mater. Sci. Process.*, 2004, **78**, 1121.
21 J. P. Zhai, I. L. Li, S. C. Ruan and Z. K. Tang, *Microporous Mesoporous Mater.*, 2009, **124**, 15.
22 B. L. Wang, Y. Mu and H. Yin, *et al.*, *Nanoscale*, 2018, **10**, 10650.
23 Y. Mu, N. Wang and Z. C. Sun, *et al.*, *Chem. Sci.*, 2016, **7**, 3564.
24 J. Cheng, G. Xiao and G. Duan, *et al.*, *Chem. Eng. J.*, 2021, **421**, 127743.
25 J. P. Zhai, Z. K. Tang and Z. M. Li, *et al.*, *Chem. Mater.*, 2006, **18**, 1505.
26 X. Li, L. Yan, J. Si, H. Xu and Y. Xu, *RSC Adv.*, 2019, **9**, 12732.
27 I. Balint, M. Springuel-Huet, K. Aika and J. Fraissard, *Phys. Chem. Chem. Phys.*, 1999, **1**, 3845.
28 H. T. Sun, Y. Matsushita and Y. Sakka, *et al.*, *J. Am. Chem. Soc.*, 2012, **134**, 2918.
29 A. Mech, A. Munguzzi and F. Cucinotta, *et al.*, *Phys. Chem. Chem. Phys.*, 2011, **13**, 5605.
30 M. C. Ortega-Liebana, N. X. Chung and R. Limpens, *et al.*, *Carbon*, 2017, **117**, 437.
31 H. Li, H. Ming and Y. Liu, *et al.*, *New J. Chem.*, 2011, **35**, 2666.
32 F. Tuinstra and J. L. Koenig, *J. Chem. Phys.*, 1970, **53**, 1126.
33 S. Niyogi, E. Bekyarova and M. E. Itkis, *et al.*, *Nano Lett.*, 2010, **10**, 4061.
34 M. S. Dresselhaus, G. Dresselhaus, R. Saito and A. Jorio, *Phys. Rep.*, 2005, **409**, 47.
35 A. C. Ferrari, *Solid State Commun.*, 2007, **143**, 47.
36 P. Kumar and H. B. Bohidar, *J. Nanopart. Res.*, 2012, **14**, 948.
37 G. Eda, Y. Y. Lin and C. Mattevi, *et al.*, *Adv. Mater.*, 2010, **22**, 505.
38 K. P. Loh, Q. L. Bao, G. Eda and M. Chhowalla, *Nat. Chem.*, 2010, **2**, 1015.